

Supplementary information

On the role of hydroxide species in sulphur- and nitrogen-doped cobalt-based carbon catalysts for the oxygen evolution reaction

Ali Sharaei, Markus Kuebler, Ioanna Martinaiou, K. Alexander Creutz, W. David Z. Wallace, Mohammad A. Nowroozi, Stephen Paul, Natascha Weidler, Robert W. Stark, Oliver Clemens, and Ulrike I. Kramm

Figure S1. Cyclic voltammetry in N_2 saturated 0.1M KOH at 100 mV s^{-1} (a) and correlation attempts of the double layer capacity with the BET surface area (b) and of the current density at 1.6 V versus micropore surface area.

Figure S2. TEM images of the catalysts at different magnifications, on top the related scaling of the scale bar is given.

Figure S3. Deconvoluted Raman spectra of the 1st order region assigned to carbon blacks for all four catalysts.

Figure S4. Correlation between I_{D3}/I_G ratio and the sum of N_{Me-N} plus $N_{pyrid.}$ and correlation between I_D/I_G ratio and the relative fraction of C-S-O (increase).

Figure S5: Co 2p full spectra range for all investigated catalysts as well as reference systems.

Figure S6: Exemplary fit of Co 2p 3/2 region of cat D with different components. The spectrum of Co_9S_8 was digitalized from data provided in Alstrup et al., J. Catalysis 1982, see reference 57 of the main manuscript.

Figure S7. Correlation of the atomic concentrations of $N_{pyridinic.}$ and C-S as a function of the S/Co ratio in the precursors.

Figure S8. The linear scan voltammograms (LSVs) and Tafel plots for evaluating the OER activity with lower catalyst loading (0.5 mg cm^{-2}) in 0.1M KOH (rpm1500).

Figure S9. Repetition of the OER activity measurements of the catalysts and standard deviation of the overpotential

Figure S10: RRDE data of the four aged catalysts measured at 10 mV s^{-1} with $5 \mu\text{l}$ ink (corresponding loading on disc: 0.412 mg cm^{-2}), the ring potential was kept at 0.45 V (SHE). Darker colors refer to the anodic (initial) scan, lighter colors to the related cathodic scan that was performed after.

Figure S11. LSVs of the most active catalyst measured at different time intervals after preparation (as indicated in the label) and plot of the overpotential versus time after preparation. It becomes visible that there is a strong decay of the catalyst with storage time.

Figure S12. Trends in faradaic efficiency as a function of applied potential for the aged catalysts A to D. See Table S1 for summary of average values at 1 mA cm^{-2} .

Figure S13. CVs during durability cycling (compare Figure 7a), shown are every 100th cycle, whereas the initial cycle, cycle No. 500 and cycle No. 2000 are highlighted in the respective color. All other cycles displayed in black. Cycling in 0.1M KOH at 1500 rpm with a sweep rate of 300 mV s⁻¹.

Figure S14. Correlation attempts of the I_D/I_G ratio (a) and the full-width at half maximum (fwhm) of the D-band (b) versus the Tafel slopes.

Figure S15. Co 2p difference spectra of catalysts A-C in relation to the most active cat D. The arrow at ca. 778 eV might be attributed to Co-O species, whereas the arrow at ca. 782 eV is indicative of hydroxide species.

Figure S16. As-measured resistivity data (related to Figure 6 of the main manuscript) versus applied potential for the four catalysts A-D.

Figure S17: Comparison of the original activity scan of cat D and after iR correction (top graph) and comparison of the original data of all four catalysts (bottom graph). All measurements for a loading of 1 mg cm⁻².

Table S1: Summary of the faradaic efficiencies of catalysts A-D at a current density of 1 mA cm⁻² in the anodic and cathodic scan.

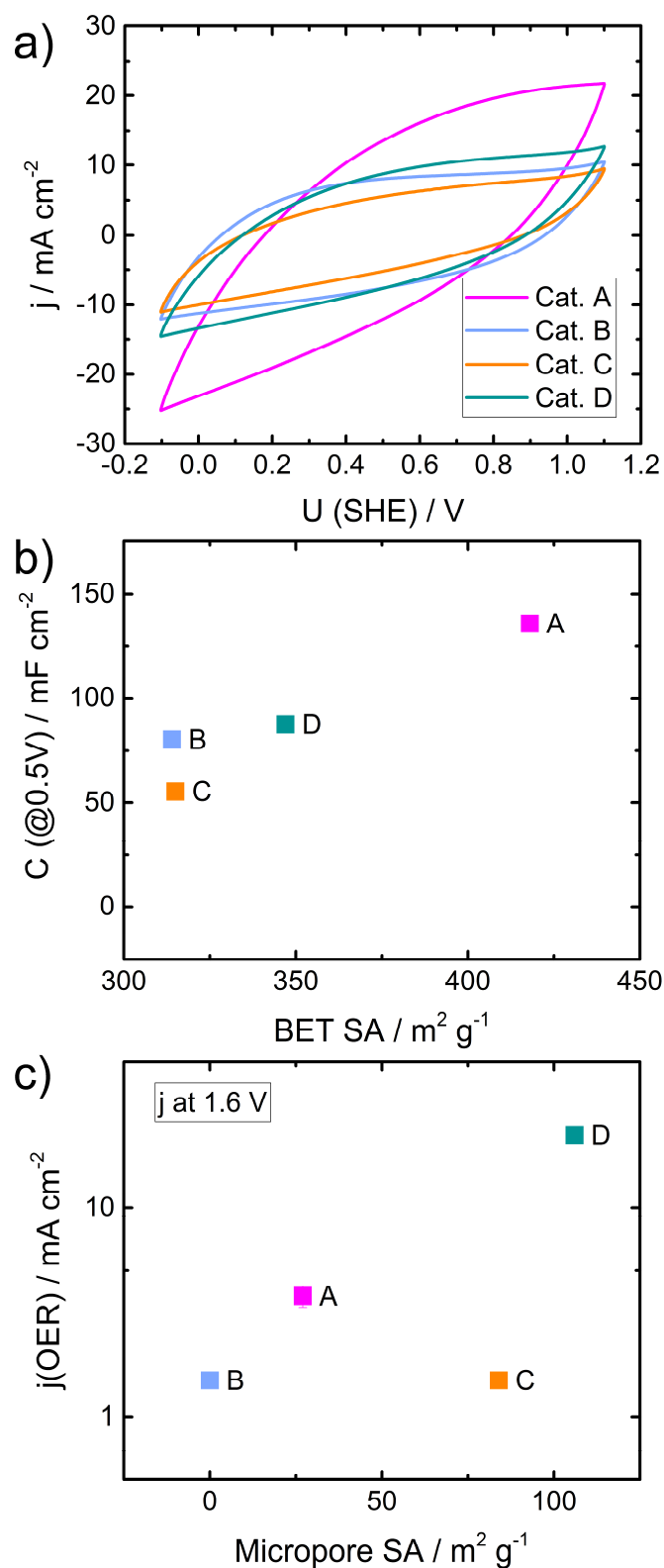


Figure S1. Cyclic voltammetry in N₂ saturated 0.1M KOH at 100 mV s⁻¹ (a) and correlation attempts of the double layer capacity with the BET surface area (b) and of the current density at 1.6 V versus micropore surface area.

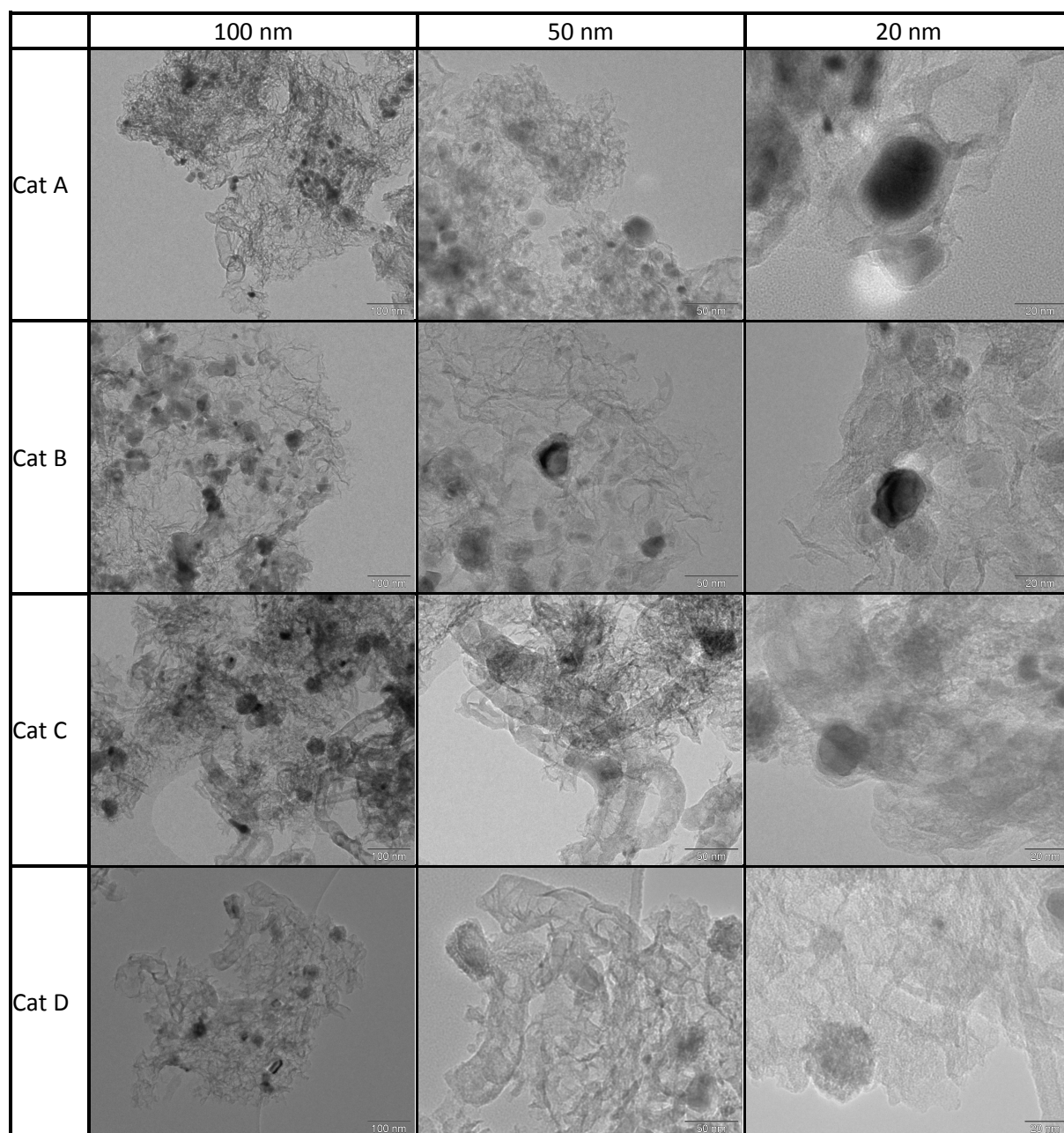


Figure S2. TEM images of the catalysts at different magnifications, on top the related scaling of the scale bar is given.

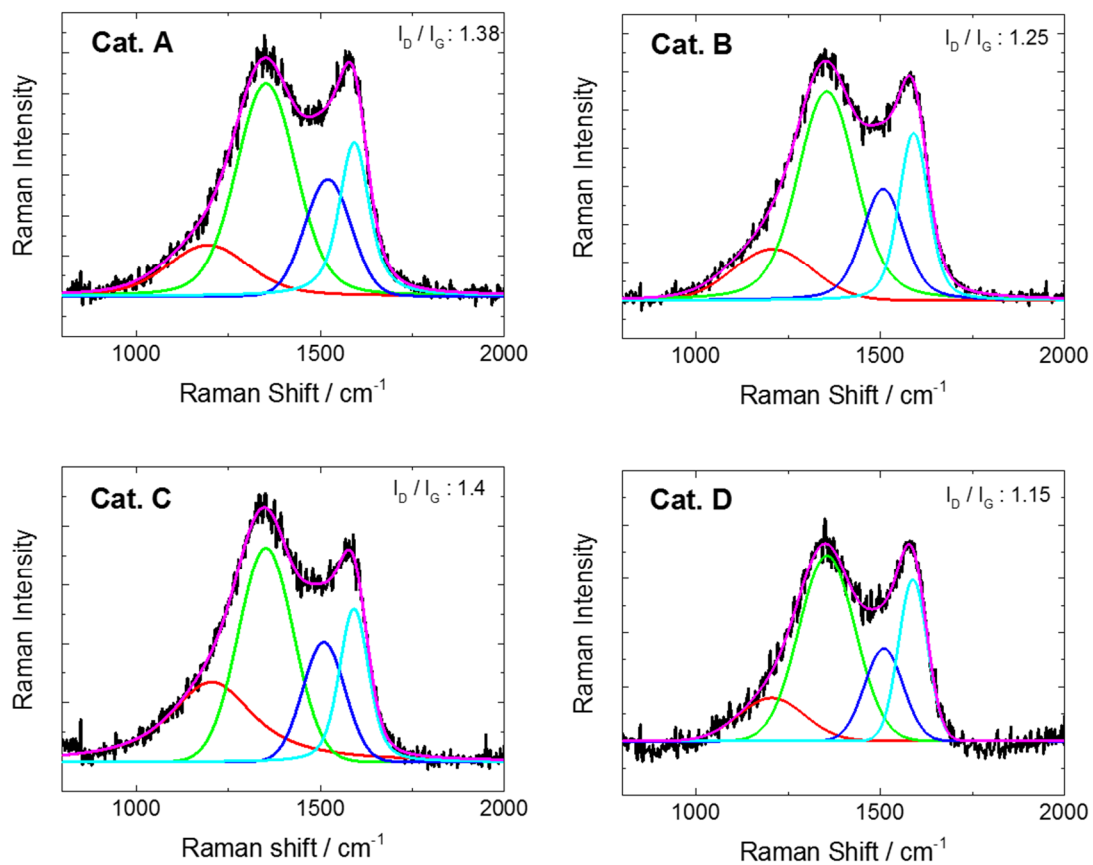


Figure S3. Deconvoluted Raman spectra of the 1st order region assigned to carbon blacks for all four catalysts.

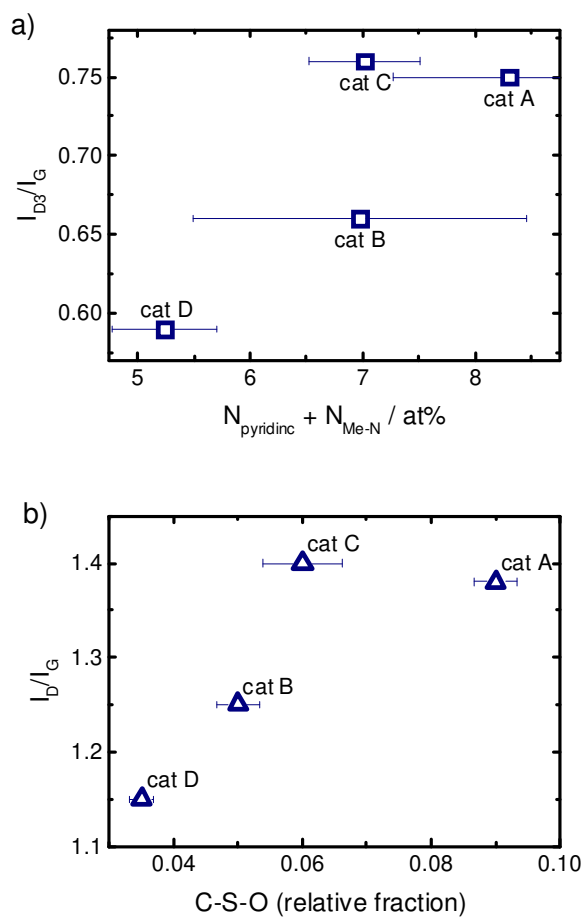


Figure S4. Correlation between I_{D3}/I_G ratio and the sum of $N_{\text{Me-N}}$ plus $N_{\text{pyrid.}}$ and correlation between I_D/I_G ratio and the relative fraction of C-S-O (increase).

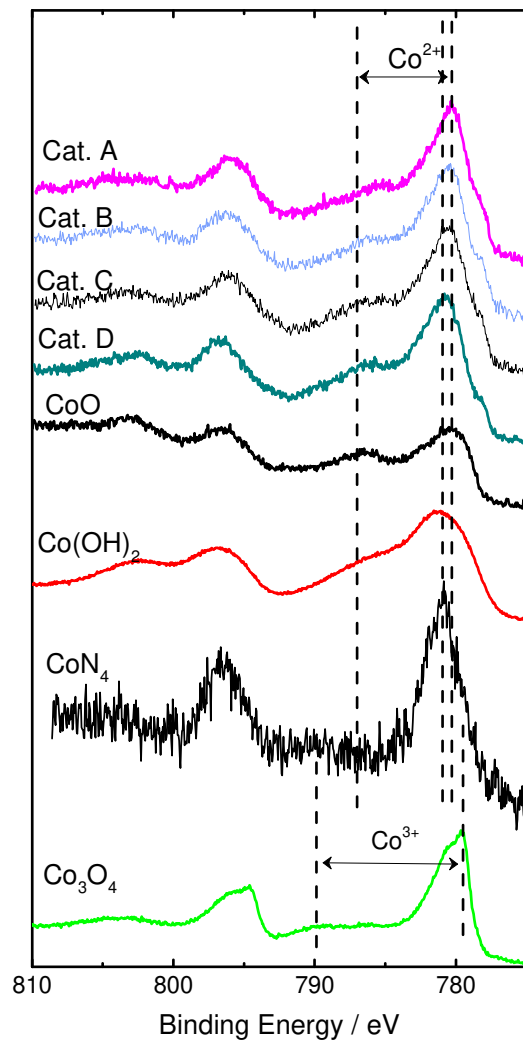


Figure S5: Co 2p full spectra range for all investigated catalysts as well as reference systems.

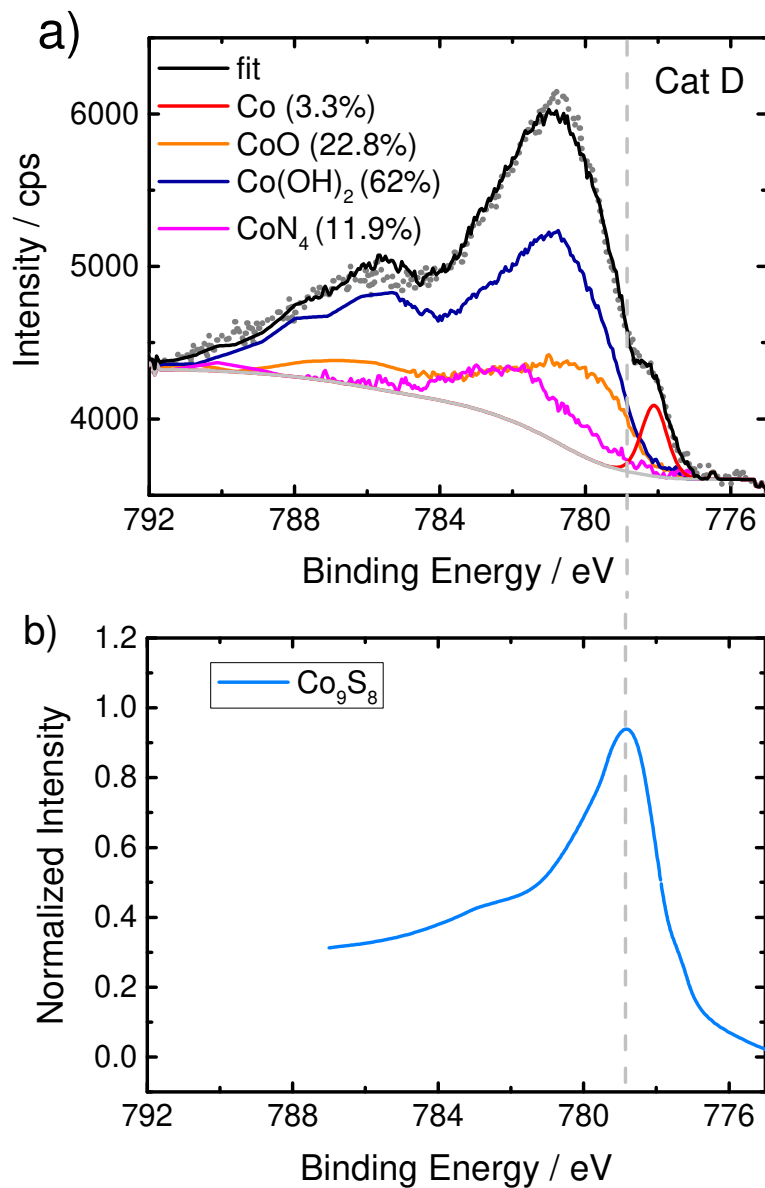


Figure S6: Exemplary fit of Co 2p 3/2 region of cat D with different components. The spectrum of Co₉S₈ was digitalized from data provided in Alstrup et al., J. Catalysis 1982, see reference 57 of the main manuscript.

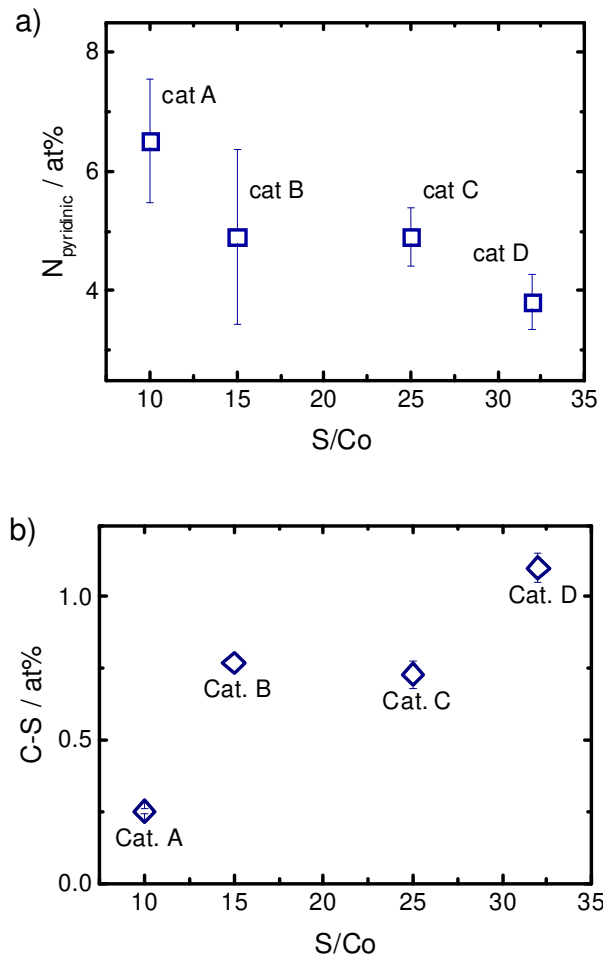


Figure S7. Correlation of the atomic concentrations of N_{pyridinic}, and C-S as a function of the S/Co ratio in the precursors.

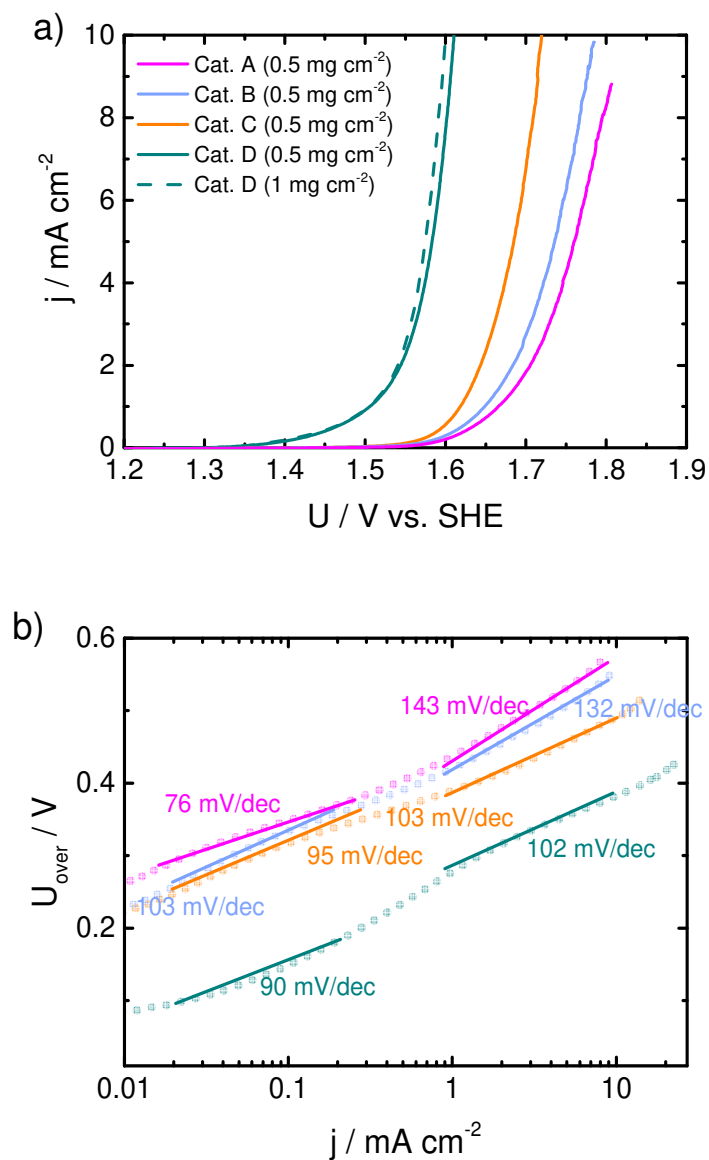


Figure S8. The linear scan voltammograms (LSVs) and Tafel plots for evaluating the OER activity with lower catalyst loading (0.5 mg cm^{-2}) in 0.1 M KOH (rpm1500).

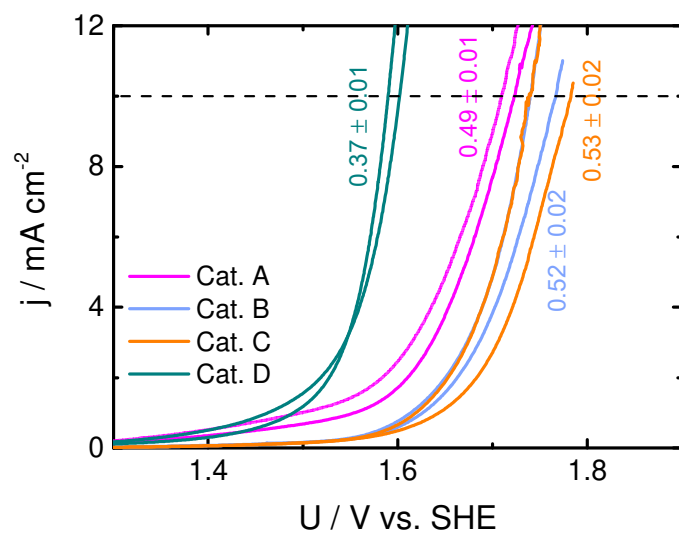


Figure S9. Repetition of the OER activity measurements of the catalysts and standard deviation of the overpotential

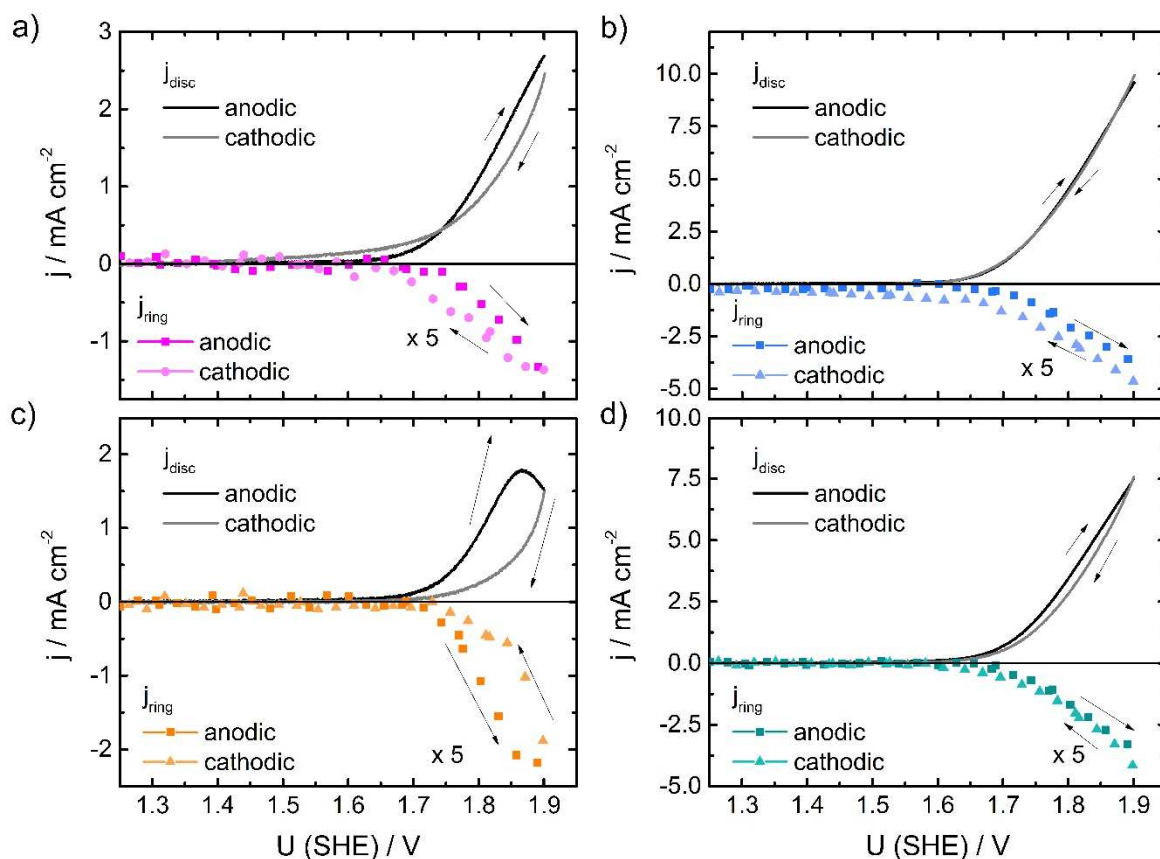


Figure S10: RRDE data of the four aged catalysts measured at 10 mV s^{-1} with $5 \mu\text{l}$ ink (corresponding loading on disc: 0.412 mg cm^{-2}), the ring potential was kept at 0.45 V (SHE). Darker colors refer to the anodic (initial) scan, lighter colors to the related cathodic scan that was performed after.

The increase of efficiency from anodic to cathodic sweep might have been caused by the decrease in the carbon oxidation contribution as it was shown for some carbon blacks that carbon oxidation decreases with number of cycles.

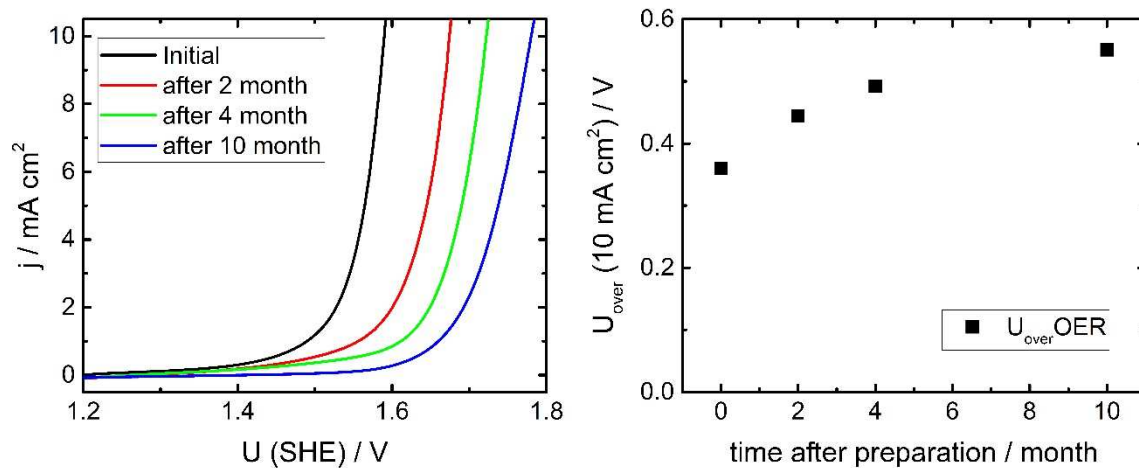


Figure S11. LSVs of the most active catalyst measured at different time intervals after preparation (as indicated in the label) and plot of the overpotential versus time after preparation. It becomes visible that there is a strong decay of the catalyst with storage time.

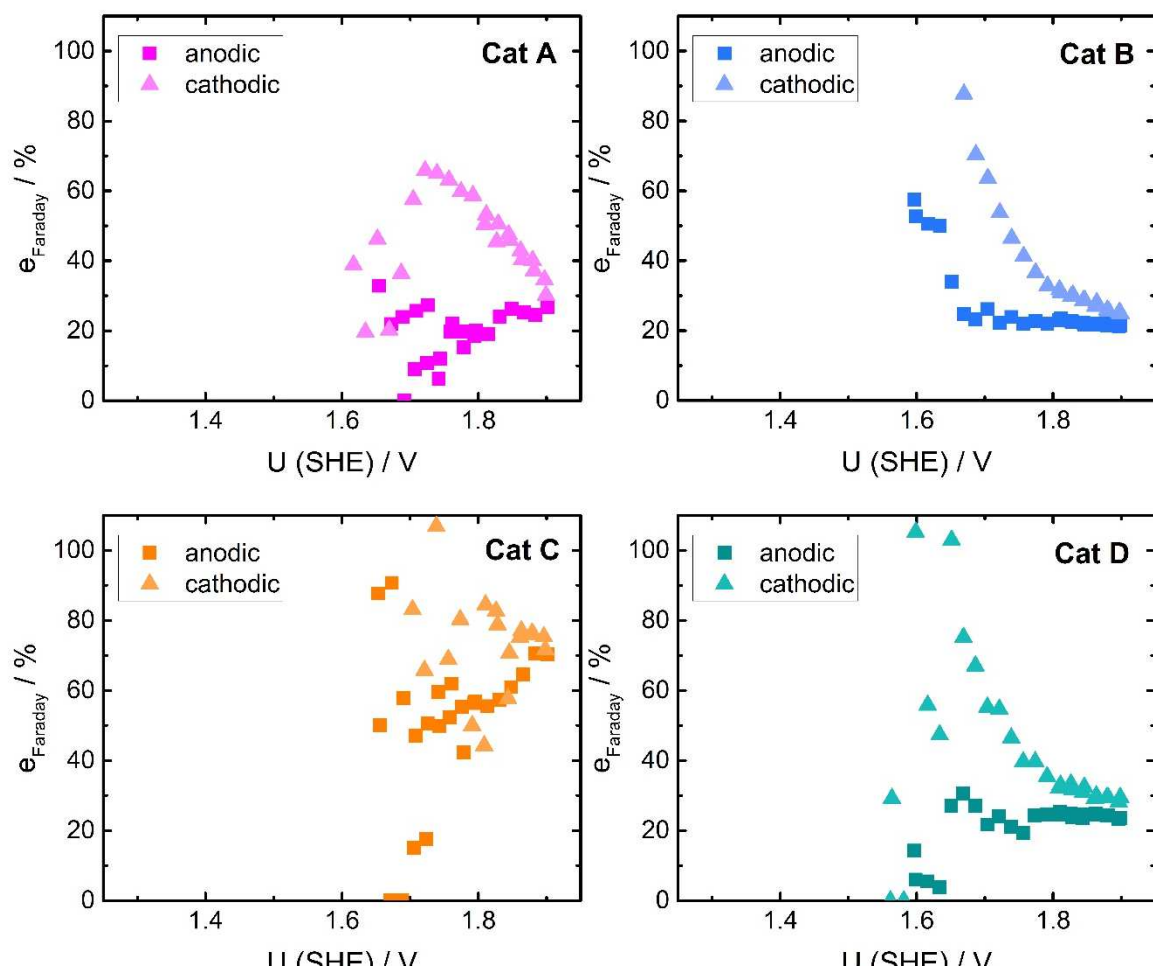


Figure S12. Trends in faradaic efficiency as a function of applied potential for the aged catalysts A to D. See Table S1 for summary of average values at 1 mA cm^{-2} .

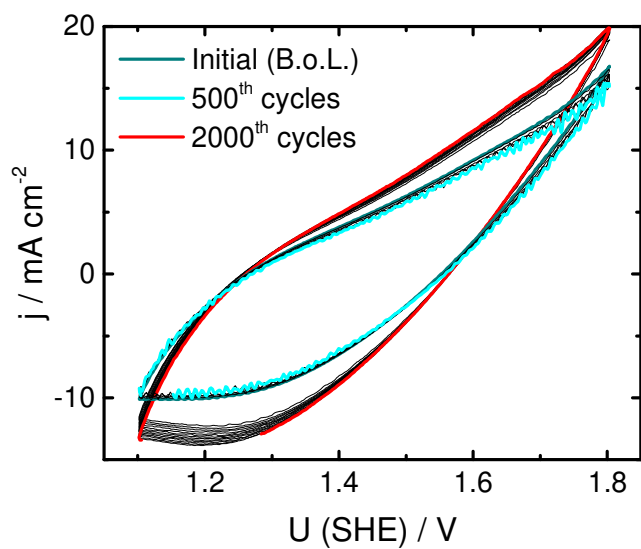


Figure S13. CVs during durability cycling (compare Figure 7a), shown are every 100th cycle, whereas the initial cycle, cycle No. 500 and cycle No. 2000 are highlighted in the respective color. All other cycles displayed in black. Cycling in 0.1M KOH at 1500 rpm with a sweep rate of 300 mV s⁻¹.

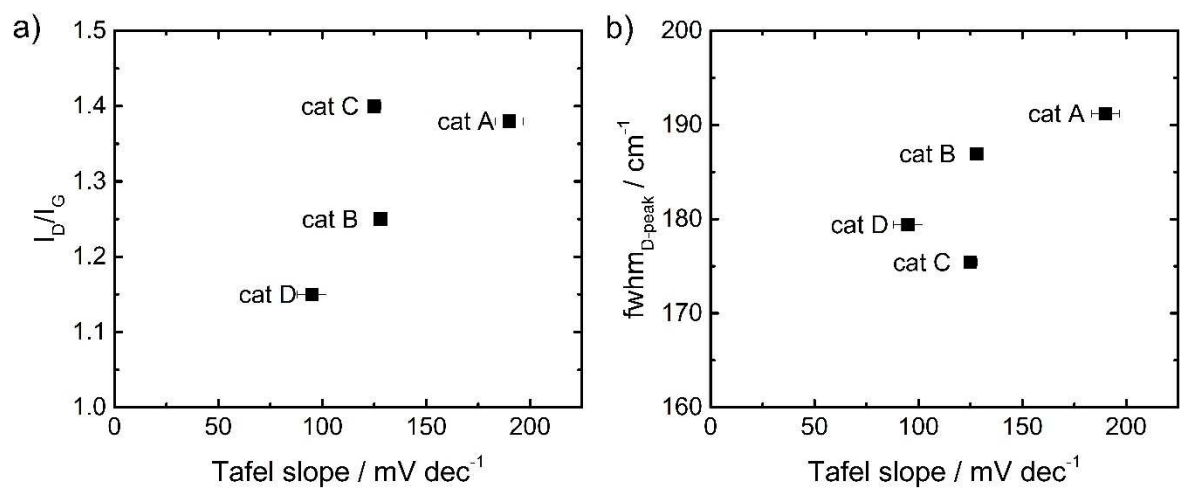


Figure S14. Correlation attempts of the I_D/I_G ratio (a) and the full-width at half maximum (fwhm) of the D-band (b) versus the Tafel slopes.

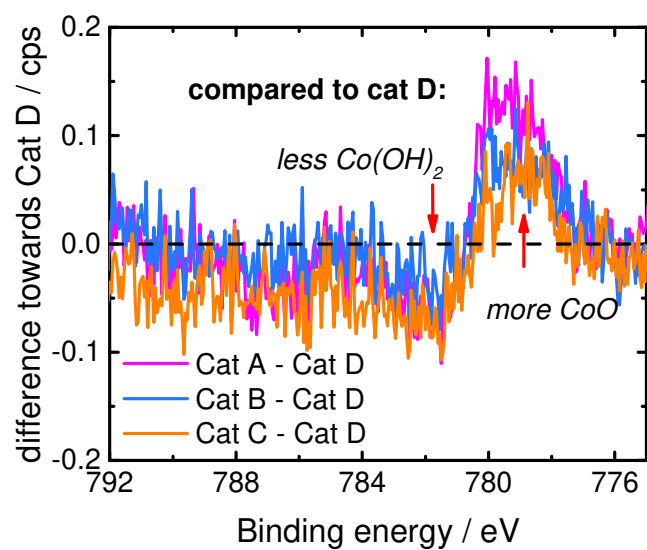


Figure S15. Co 2p difference spectra of catalysts A-C in relation to the most active cat D. The arrow at ca. 778 eV might be attributed to Co-O species, whereas the arrow at ca. 782 eV is indicative of hydroxide species.

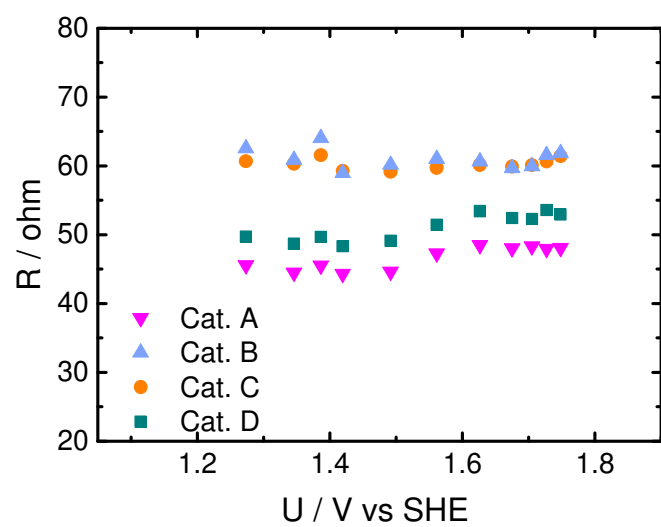


Figure S16. As-measured resistivity data (related to Figure 6 of the main manuscript) versus applied potential for the four catalysts A-D.

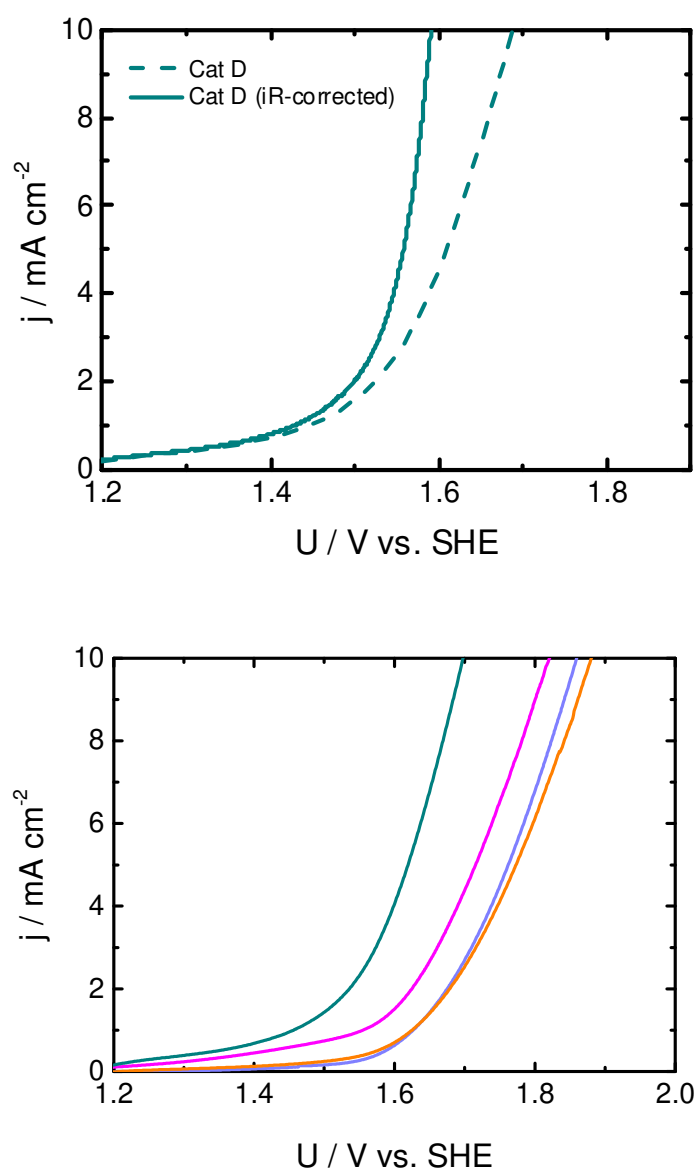


Figure S17: Comparison of the original activity scan of cat D and after iR correction (top graph) and comparison of the original data of all four catalysts (bottom graph). All measurements for a loading of 1 mg cm^{-2} .

Table S1: Summary of the faradaic efficiencies of catalysts A-D at a current density of 1 mA cm⁻² in the anodic and cathodic scan.

$\epsilon_{\text{Faraday}} / \%$	Cat A	Cat B	Cat C	Cat D
Anodic	20 ± 1	21 ± 2	55 ± 3	24 ± 1
Cathodic	49 ± 4	68 ± 2	77 ± 1	49 ± 3
Average	35	44	66	36

For the efficiency determination all values in the range 0.9 – 1.1 mA cm⁻² were considered to determine the average and standard deviation.